ISSN 0915-633X

NATIONAL INSTITUTE FOR FUSION SCIENCE

Line Statistics: Stretching Rate of Passive Lines in Turbulence

S. Kida and S. Goto

(Received - Feb. 6, 2001)

NIFS-684 Mar. 2001

RESEARCH REPORT
NIFS Series

TOKI, JAPAN

Line Statistics : Stretching Rate of Passive Lines in Turbulence

Shigeo KIDA and Susumu GOTO

Theory and Computer Simulation Center, National Institute for Fusion Science, 322-6 Oroshi-cho, Toki, 509-5292, Japan

Abstract

Passive lines in a statistically stationary isotropic incompressible turbulent flow are tracked numerically. The line length increases exponentially in time as $\exp[\gamma t]$ with the stretching rate $\gamma = 0.17$ (Kolmogorov time)$^{-1}$ which is larger, by about 30%, than the value estimated before by the arithmetic mean of the contributions from many passive vector elements. The underestimation in previous studies is attributed to the negligence of non-uniform probability weight due to non-uniform line stretching. If the effects of non-uniformity are taken into account, the true stretching rate is recovered in the early stage of evolution up to several Kolmogorov times. Thereafter, however, it is overestimated owing to the continual separation of initially adjacent vector elements.

Keywords: passive (material) lines, stretching, mixing, turbulence

1 Introduction

It is fundamental in mixing and diffusion problems to understand how physical quantities accompanied with fluid elements are transported in turbulent flows. Because of complexity of turbulent motions the measurements using passively floating particles have been frequently used as convenient tools for effective estimations of various transport coefficients as well as the convoluted velocity field itself. The particle tracking velocimetry [1] is one of the typical examples. An important point to notice here is that there is an implicit premise that each particle is statistically equivalent. In other words, the histogram of velocity, for example, is obtained by equi-weight contributions from all the particles in a homogeneous flow. This is true for an incompressible flow so long as the statistics over the three-dimensional space are concerned since the number density is invariant in time. This is the Lagrangian volume statistics.

It is *not* true, however, for statistics on passive (or material) lines or passive surfaces [2], which we call the Lagrangian line statistics and the Lagrangian surface statistics, respectively. This is because the flow is not incompressible in one- or two-dimensional objects even if it is *three-dimensionally* incompressible. If a flow is statistically homogeneous in space and stationary in time, and particles are assumed to migrate uniformly over some flow domain (the uniform mixing hypothesis), then the Lagrangian volume average may be equivalent to the average taken over this domain. The latter is the Eulerian volume statistics. Hereafter, the adjective "Lagrangian" in front of the line, the surface, and the volume statistics, etc. will be omitted for brevity.

In this paper we focus our attention on the difference between the line average and a thin limit of the volume average, which has been sometimes overlooked in estimation of the stretching rate of passive lines in turbulence to give rise to substantial underestimation [3, 4]. In the next section two similar but different thin limits of the volume averages are introduced. The stretching rate of passive lines in turbulence is investigated in Sec. 3. After describing the numerical simulation of the motion of a passive line in turbulence, we present the traditional and our new averages of the stretching rate of passive lines, and examine their difference in the statistics of the rate-of-strain tensor, where the role of non-uniformity of line stretching is emphasized. Section 4 is devoted to concluding remarks.

2 Line and Thin-Tube Averages

The mean value of a physical quantity $F(\boldsymbol{x}, t)$ associated with a blob of fluid elements is expressed by the conditional average,

$$\langle F \rangle_{\rm vol} = \frac{1}{V_t} \int_{V_t} F(\boldsymbol{x}, t)\, {\rm d}V, \tag{1}$$

where the integration is taken over the blob of volume V_t. Hereafter, the subscript t denotes the time. This is called the *volume average*. The shape of the blob generally changes in time but the volume is invariant in an incompressible flow. The mean value of $F(\boldsymbol{x}, t)$ on a fluid line is defined by

$$\langle F \rangle_{\rm line} = \frac{1}{L_t} \int_{L_t} F(\boldsymbol{x}, t)\, {\rm d}L, \tag{2}$$

where the integration is carried out over the whole line of length L_t. This is called the *line average*.

This average is expressed by a thin limit of the volume average over a uniform circular tube which includes the line as

$$\langle F \rangle_{\text{line}} = \lim_{\text{dia}(V_t)\to 0} \frac{1}{V_t} \int_{V_t} F(\boldsymbol{x}, t)\, \mathrm{d}V, \qquad (3)$$

where $\text{dia}(V_t)$ denotes the diameter of the tube. Another thin limit of volume average, which is called the *thin-tube average*, is defined by

$$\langle F \rangle_{\text{tube}} = \lim_{\text{dia}(V_0)\to 0} \frac{1}{V_t} \int_{V_t} F(\boldsymbol{x}, t)\, \mathrm{d}V, \qquad (4)$$

where $\text{dia}(V_0)$ denotes the diameter of a uniform circular tube V_0 at an earlier time t_0 ($< t$) of the domain V_t over which the average is taken.

It is important to note that the line average and the thin-tube average are different in general, i.e.

$$\langle F \rangle_{\text{line}} \neq \langle F \rangle_{\text{tube}}. \qquad (5)$$

This may be understood most easily with reference to figure 1 which illustrates that a uniform tube V_0 submerged at an initial time t_0 is advected in an incompressible flow to change into a deformed tube V_t with non-uniform cross-section at a later time t. In this example the tube is being pinched in the right part where it is stretched most strongly along the axis. The difference between the above two averages is clear if only we remember that the thin-tube average is the thin limit of the volume average over this deformed tube, whereas the line average is the thin limit of the volume average over a uniform tube (figure 1(c)) around the center line at time t. The contribution from narrow parts of the deformed tube to the thin-tube average tends to be smaller than others. In contrast, any part of the line contributes to the line average with an equal probability weight. Note that the effects of this non-uniformity remain even in the limit of vanishing diameter of the initial uniform tube V_0. Those particles chosen with equal distance apart at the initial time (figure 1(a)) are redistributed non-uniformly in the tube at a later time because of non-uniform stretching (figure 1(b)). The thin-tube average is obtained by taking the contribution from each particle with equal weight. If, on the other hand, the effects of the non-uniform stretching are taken into account, i.e. if the contribution from a particle is weighted by a factor proportional to the distance between the neighboring particles, the line average is recovered under the condition that the particles are sufficiently dense. The importance of this proviso will be clarified in Sec. 3.6.

The non-uniform weight due to non-uniform stretching should be kept in mind whenever statistics are considered on a passive line. The difference between these two averages is especially important for such quantities that depend strongly on the line stretching (Sec. 3.7).

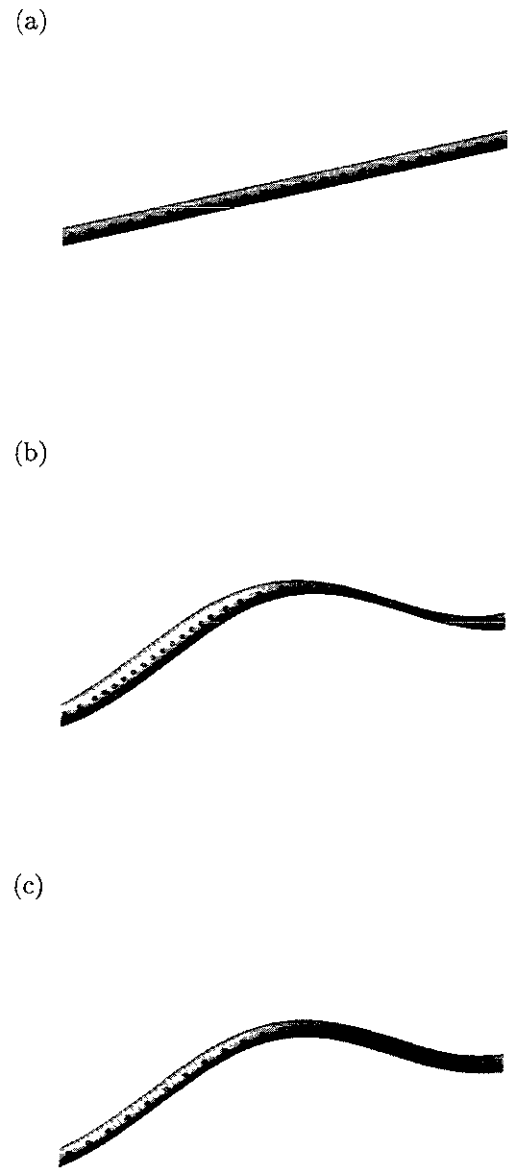

Figure 1 Non-uniform stretching. (a) A uniform circular tube picked up at some initial time in an incompressible flow is deformed into (b) a non-uniform tube without changing its volume. The initial center line is deformed and stretched in general. Those passive particles located with equal distance apart on the center line at the initial time are redistributed non-uniformly at a later time. The particles are more separated at thinner parts of the tube. (c) A new uniform circular tube with the same centerline as in (b).

3 Stretching of Passive Lines

As a typical example of the line statistics we consider the stretching of passive lines advected in a turbulent flow. This phenomenon is of practical importance in relation to turbulent mixing and diffusion. The stretching rate has already been investigated by many authors [3, 4] numerically. Instead of tracking passive lines they evaluated it by taking the arithmetic mean over a number of passive vector elements. This may correspond to the thin-tube average introduced in Sec. 2. Unfortunately, however, this method leads to a substantial underestimation of the stretching rate owing to the negligence of the effects of the non-uniform probability weight caused by non-uniform stretching stated in the preceding section. Here, instead, we calculate, by the line average, the correct stretching rate, and compare it with the values determined by the thin-tube average. The reason of the discrepancy between these two averages will be clarified in the subsequent sections.

3.1 Numerical Turbulence

The turbulent velocity field $\boldsymbol{u}(\boldsymbol{x},t)$ which we analyze here is governed by a forced incompressible Navier-Stokes equation,

$$\frac{\mathrm{D}}{\mathrm{D}t}\,\boldsymbol{u}(\boldsymbol{x},t) = -\frac{1}{\rho}\,\nabla p(\boldsymbol{x},t) + \nu\,\nabla^2\,\boldsymbol{u}(\boldsymbol{x},t) + \boldsymbol{f}(\boldsymbol{x},t) \quad (6)$$

supplemented by the continuity equation,

$$\nabla\cdot\boldsymbol{u}(\boldsymbol{x},t) = 0, \quad (7)$$

where

$$\frac{\mathrm{D}}{\mathrm{D}t} = \frac{\partial}{\partial t} + \boldsymbol{u}(\boldsymbol{x},t)\cdot\nabla \quad (8)$$

is the Lagrangian (or material) derivative, $p(\boldsymbol{x},t)$ is the pressure, ρ is the constant density, and ν is the kinematic viscosity. A forcing term $\boldsymbol{f}(\boldsymbol{x},t)$ is imposed in order to keep the flow statistically stationary.

The set of equations (6) and (7) is solved numerically in a periodic cube with period 2π starting with some appropriate initial condition, the detailed structure of which is irrelevant to the statistics in the statistically stationary state which will be dealt with in this paper. The Fourier spectral method of resolution N^3 is employed for spatial derivatives and the Runge-Kutta-Gill scheme for time derivatives. The aliasing interactions are eliminated by the phase shift method so that the maximum wavenumber $k_{\max}$ retained in the simulation is $0.47N$. The amplitude of Fourier modes at lower wavenumbers ($|\boldsymbol{k}| \le k_f$) is kept constant at all the time, while their phases are allowed to evolve freely as the equations of motion permit. This is one of the effective forcing schemes which keep the flow field statistically stationary with minimal contamination effects to the small-scale motions.

The simulation is performed with resolution $N^3 = 128^3$ (hence, the grid width $\Delta x = 2\pi/N = 0.049$), the viscosity $\nu = 0.005$, and the time step width $\Delta t = 0.01$. The amplitudes of the Fourier coefficients of vorticity of wavenumbers less than or equal to $k_f = \sqrt{8}$ are set at 0.1. The turbulent flow field gets in the statistically stationary state after several eddy-turnover times. Thereafter the Taylor micro-scale Reynolds number,

$$R_\lambda = \sqrt{\frac{20}{3\nu\,\epsilon}}\,\mathcal{E} \quad (9)$$

achieves 56 in the temporal mean, where $\mathcal{E}$ is the spatial mean turbulent energy per unit mass and ϵ is the spatial mean energy dissipation rate. The Kolmogorov length $\eta = \nu^{\frac{3}{4}}\epsilon^{-\frac{1}{4}}$ and the Kolmogorov time $\tau_\eta = \epsilon^{-\frac{1}{2}}\nu^{\frac{1}{2}}$ fluctuate around $\overline{\eta} = 0.032$ ($= 0.65\Delta x$) and $\overline{\tau}_\eta = 0.20$ ($= 20\Delta t$), respectively, where an overbar denotes the temporal mean. The product $k_{\max}\,\overline{\eta}$ serves as a measure of the numerical accuracy to assess whether the smallest active motions are well resolved or not. It amounts to 1.91 which is well above the commonly accepted tolerable value of 1.5.

3.2 Evolution of Passive Lines

We simulate numerically the motion of a passive line advected in a fully developed turbulent flow described in the preceding section. The passive line is represented by a chain of short segments. Let I_t be the number of the segments. The i-th segment ($i = 1, 2, \cdots, I_t$) has two nodes $\boldsymbol{x}_t^{(i-1)}$ and $\boldsymbol{x}_t^{(i)}$ which are advected by the local velocity as

$$\frac{\mathrm{d}\boldsymbol{x}_t^{(i)}}{\mathrm{d}t} = \boldsymbol{u}(\boldsymbol{x}_t^{(i)},t) \qquad (i = 0, 1, 2, \cdots, I_t)\,. \quad (10)$$

The i-th segment vector,

$$\boldsymbol{l}_t^{(i)} = \boldsymbol{x}_t^{(i)} - \boldsymbol{x}_t^{(i-1)} \qquad (i = 1, 2, \cdots, I_t)\,, \quad (11)$$

then changes in time as

$$\frac{\mathrm{d}\boldsymbol{l}_t^{(i)}}{\mathrm{d}t} = \boldsymbol{u}(\boldsymbol{x}_t^{(i)},t) - \boldsymbol{u}(\boldsymbol{x}_t^{(i-1)},t) \qquad (i = 1, 2, \cdots, I_t)\,. \quad (12)$$

The motion of a passive line is tracked by solving (6), (7) and (10) simultaneously. In this simulation the right-hand side of (10) is calculated by the 4^3-point Lagrangian interpolation in terms of the velocity field at the grid points. The time step width is taken as $\Delta t = 0.01$ for (6) and (7) and $\Delta t = 0.02$ for (10). The segments generally get longer in time. The length of each segment is always kept below a given threshold, say $1.5\Delta x$, to guarantee the numerical accuracy. That is, whenever a segment exceeds this threshold, a new

node is inserted at the center of the segment and the total number I_t of the segments increases by one.

A straight line of the length L_0 ($= 2\pi$) is submerged in a fully developed turbulent flow, at which the origin of time is set up in the following discussion. Snapshots of the passive line at four time instants are drawn at every $10\overline{\tau}_\eta$ in figure 2. As time progresses, the line is getting longer rapidly, more convoluted, and fills up quickly the whole flow field apparently uniformly. The total length L_t of the line increases by 5.5 times every $10\overline{\tau}_\eta$ (see (15) below). The sum of the lengths $l_t^{(i)} = |\boldsymbol{l}_t^{(i)}|$ ($i = 1, 2, \cdots, I_t$) of the constituent segments yields the total length of the line as

$$L_t = \sum_{i=1}^{I_t} l_t^{(i)} , \tag{13}$$

the temporal evolution of which is plotted in figure 3. A nearly straight line in this semi-logarithmic plot indicates that the length increases exponentially in time as

$$L_t = L_0 \exp\Big[\, \gamma_L \, t \,\Big]. \tag{14}$$

The mean stretching rate γ_L read from the slope of this line is

$$\gamma_L = \frac{\mathrm{d}}{\mathrm{d}t} \ln L_t = 0.17\, \overline{\tau}_\eta^{-1} . \tag{15}$$

Note that this value of γ_L estimated from the total length of a passive line should be the *true* stretching rate.

In the following sections the stretching rate of passive lines is estimated by the averages over passive vector elements with and without non-uniform probability weight factor (Secs. 3.3 and 3.6) as well as by the line average (Sec. 3.4). Among these three averages, only the line average gives the correct results. The difference between the line and the thin-tube (i.e., the simple volume) statistics of the rate-of-strain tensor which determines directly the stretching rate of passive lines will be discussed in Sec. 3.7.

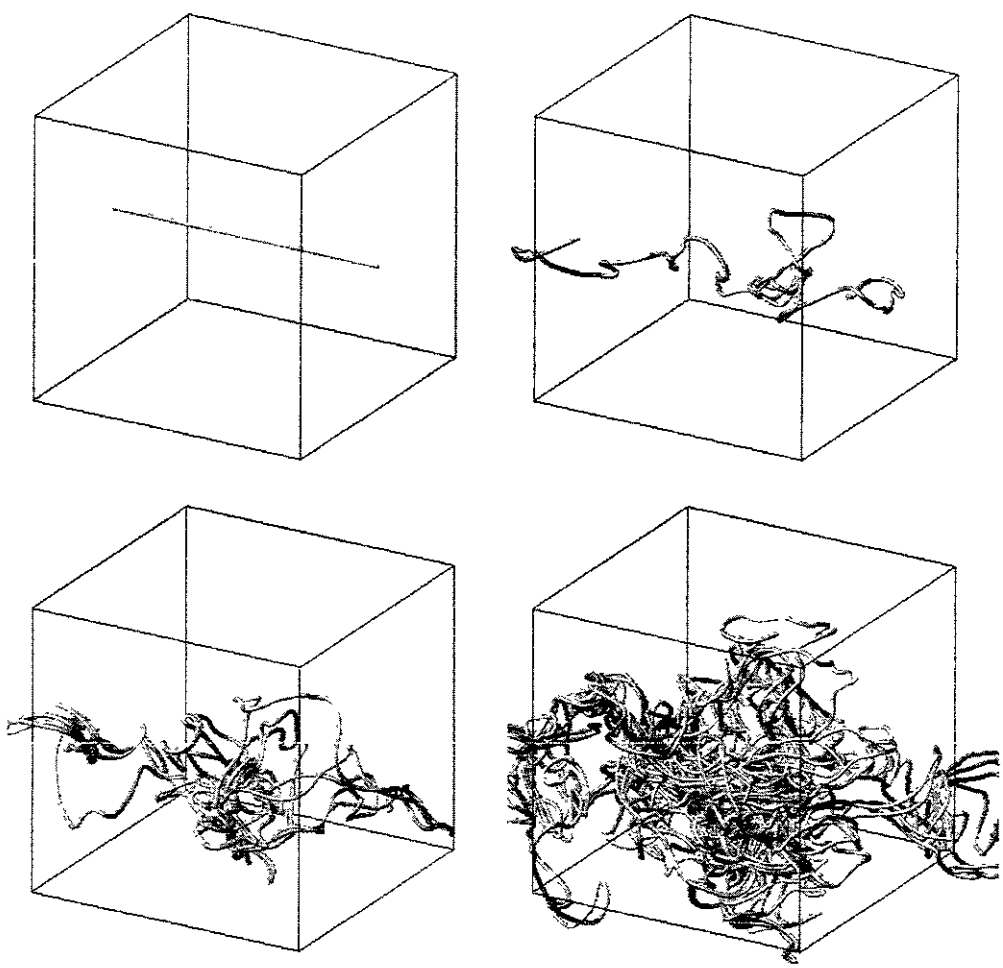

Figure 2 Temporal evolution of a passive line. (a) $t/\overline{\tau}_\eta = 0$, (b) 10, (c) 20, and (d) 30. The total length increases by 5.5 times every $10\,\overline{\tau}_\eta$.

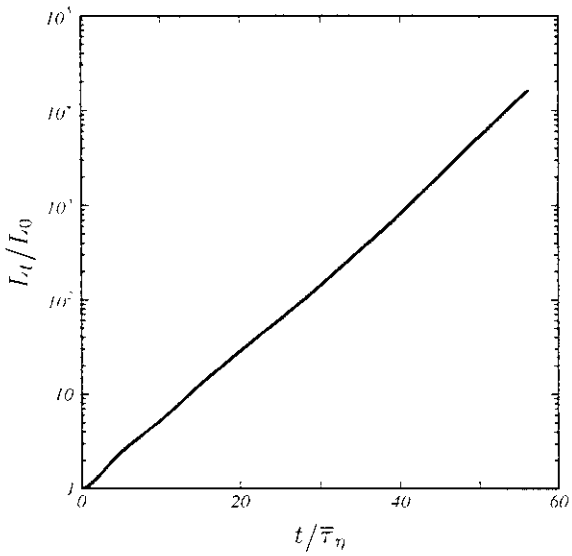

Figure 3 Exponential stretching of a passive line. The length of the line is normalized by the initial length, and the time by the Kolmogorov time $\bar{\tau}_\eta$. The straight line in this semi-logarithmic scale indicates that the length increases exponentially in time as $L_t/L_0 = \exp\left[\, 0.17 t/\bar{\tau}_\eta \,\right]$.

3.3 Simple Volume Average

The rapid development of complexity and uniformanization of a passive line advected in a turbulent flow shown in figure 2 suggests such an idea (though erroneous) that the line average might be evaluated most easily by the arithmetic mean of contributions from many passive vector elements * $\delta\boldsymbol{l}(\boldsymbol{x},t)$ distributed uniformly over the entire velocity field [3, 4]. Their temporal evolutions are governed by

$$\frac{\mathrm{D}}{\mathrm{D}t}\,\delta\boldsymbol{l}(\boldsymbol{x},t) = \left(\delta\boldsymbol{l}(\boldsymbol{x},t)\cdot\nabla\right)\boldsymbol{u}(\boldsymbol{x},t)\,. \tag{16}$$

The stretching rate $\gamma_{\delta l}$ of a vector element $\delta\boldsymbol{l}$ is expressed in term of the rate-of-strain tensor $\underline{\boldsymbol{S}}(\boldsymbol{x},t)$, the symmetric part of the velocity gradient tensor $\nabla\boldsymbol{u}$, as

$$\gamma_{\delta l} = \frac{\mathrm{D}}{\mathrm{D}t}\,\ln\,\delta l = \frac{\delta\boldsymbol{l}\cdot\underline{\boldsymbol{S}}\cdot\delta\boldsymbol{l}}{\delta l^2}. \tag{17}$$

where $\delta l = |\delta\boldsymbol{l}|$. This equation shows that the stretching rate is of the order of the rate-of-strain tensor, which is $O(\bar{\tau}_\eta^{-1})$ according to Kolmogorov's dimensional analysis.

Equation (16) together with (6) and (7) is solved for the vector elements which leave at all the grid points. (Instead of (16) we actually solve (12) with each segment length being kept as Δx.) This kind of simulation is called the passive-vector-element simulation in order to distinguish from the line simulation described in the preceding section. We investigate two typical cases of different initial conditions. In the first case the directions of the initial vector elements are aligned in parallel to a row of the grid points, whereas in the second they are distributed randomly and isotropically. The former is considered as a sort of line simulations of many straight passive lines, in which any new interpolated segments are not inserted so that the lines are composed only of the initial segments. Hence, the arithmetic mean of (17) over all the elements (i.e., the volume average) can be regarded as the stretching rate in the thin-tube average (see Sec. 2). Furthermore, the volume average is expected to be independent of the initial condition at sufficiently later times under the uniform mixing hypothesis that each vector element tends to migrate uniformly over the entire flow field with unpredictable directions in the course of evolution.

The temporal evolutions of the stretching rates obtained by the above volume average are plotted in figure 4(a). The mean and the standard deviation over ten different turbulent flows, i.e. over $10 \times N^3$ vector elements are represented by solid lines and gray zones, respectively. A thick and a thin curves refer to the mean values for the parallel and the random initial directions of vector elements, respectively. The mean stretching rate in the former is larger than that in the latter at earlier times (invisible in this figure †), but the initial condition dependence is lost and the two cases are indistinguishable after a few Kolmogorov times. The time average over $20 \le t/\bar{\tau}_\eta \le 90$ of the mean value of the stretching rate is

$$\langle\gamma\rangle_{\mathrm{vol}} = (0.13 \pm 0\,01)\,\bar{\tau}_\eta^{-1}, \tag{18}$$

where $\pm$ denotes the standard deviation over the ten different flows. Both of the mean and the standard deviation hardly change in time, i.e. they are in the statistically stationary state after $10\,\bar{\tau}_\eta$ approximately.

The value of (18) is comparable with $0.13 \sim 0.14$, the one obtained before by essentially the same calculations [3, 4]. It is, however, substantially smaller than the true stretching rate (15) obtained directly by the time-derivative of the total line length. This surprising discrepancy will be examined in the following sections.

---

*Here, a vector element implies a segment vector of infinitesimal length.

†It is conjectured that the mean stretching rate in the thin-tube average is the largest of all the volume average.

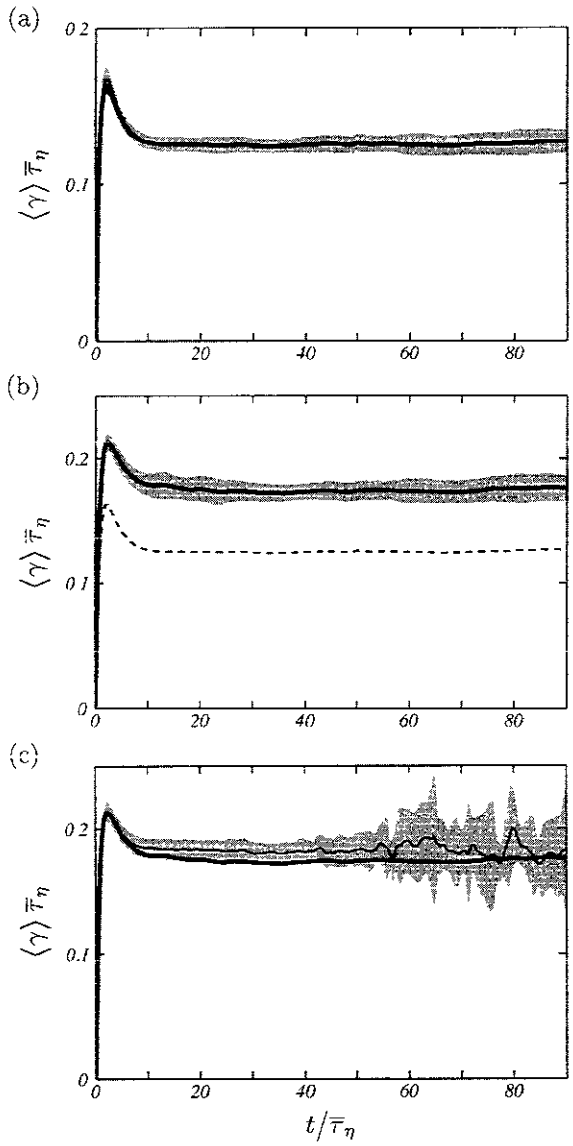

Figure 4 Stretching rate of passive lines. The time t and the stretching rate γ are normalized by the mean Kolmogorov time $\overline{\tau}_\eta$ and its reciprocal, respectively. Gray zones denote the standard deviations over 10 (in (a) and (b)) or 25 (in (c)) different turbulent flows. (a) Initial condition dependence of simple volume average. A thick and a thin curves denote the stretching rate for the cases of parallel and random initial directions of vector elements, respectively. After a few $\overline{\tau}_\eta$, the two curves get indistinguishable, implying that the initial condition dependence has been lost by this time. (b) Comparison between the line average (thick curve) and the thin-tube (or volume) average (dashed curve). The thin-tube average underestimates the stretching rate by 24%. (c) Comparison between the weighted volume average (thin curve) and the line average (thick curve). The two curves agree excellently with each other only at the early stage of evolution ($t < 0.8\overline{\tau}_\eta$).

3.4 Line Average

In the line simulation described in Sec. 3.2 each segment is halved every time it becomes longer than a threshold ($1.5\Delta x$). The number of times of divisions is generally different from segment to segment depending on the total amount of stretching of each segment undergone during the evolution. A segment has been divided into 2^m pieces after m divisions. Let M be the maximum number of divisions of each segment done by time t, and let us imagine that the I_0 initial segments of length l_0 be divided into 2^M pieces of length l_0^* ($= 2^{-M} l_0$). Then the present simulation is essentially the same at least up to t as the one in which a passive line is composed of I^* ($= 2^M I_0$, which is fixed in time) segments with initial length l_0^*. The total length of the line is expressed by

$$L_t = \sum_{j=1}^{I^*} l_t^{*(j)} \,. \tag{19}$$

The time derivative of the logarithm of (19) yields the stretching rate of a passive line L_t as

$$\gamma_{\rm L} = \frac{1}{L_t} \sum_{j=1}^{I^*} \gamma_t^{*(j)} \, l_t^{*(j)} \,, \tag{20}$$

where

$$\gamma_t^{*(j)} = \frac{{\rm d} \ln l_t^{*(j)}}{{\rm d}t} \qquad (j = 1, 2, \cdots, I^*) \tag{21}$$

is the stretching rate of $l_t^{*(j)}$. In terms of those segments $l_t^{(i)}$ ($i = 1, 2, \cdots, I_t$) actually used in the simulation, the summation (20) may be written as

$$\gamma_{\rm L} = \frac{1}{L_t} \sum_{i=1}^{I_t} \gamma_t^{(i)} \, l_t^{(i)} = \langle\gamma\rangle_{\rm line} \,, \tag{22}$$

where

$$\gamma_t^{(i)} = \frac{{\rm d} \ln l_t^{(i)}}{{\rm d}t} \qquad (i = 1, 2, \cdots, I_t) \tag{23}$$

is the stretching rate of $l_t^{(i)}$. In the derivation of (22) we have noticed that a single segment $l_t^{(i)}$ ($i = 1, 2, \cdots, I_t$) with the stretching rate $\gamma_t^{(i)}$ is composed of $j_i - j_{i-1}$ segments $l_t^{*(j)}$ ($j = j_{i-1} + 1, \cdots, j_i$, where $j_0 (= 0) < j_1 < j_2 < \cdots < j_{I_t} (= I^*)$) with the same stretching rate $\gamma_t^{*(j)} = \gamma_t^{(i)}$. The second equality of (22) states that the summation approximates the line integral (2). It should be stressed that the line average is not calculated by a simple sum (as in the thin-tube average, see Sec. 2) of the stretching rate of the segments but by a weighted sum multiplied by the segment length.

The expression (22) is employed here for the numerical calculation of the stretching rate. Initially, N^2 straight lines are placed orderly which are parallel to a row of the grid points and separated by the grid width. Each line has N nodes, all of which are put on the grid

points. This is exactly the same initial condition as that used in the passive-vector-element simulation with parallel initial vector elements analyzed in the preceding section. The number of nodes may increase indefinitely because of ever stretching of lines. In order to fix the number of sample points, each line is chopped so that the number of nodes may always be equal to the initial value N. This chopping of lines should not change the statistics because of the flow field is homogeneous. The above simulation was repeated ten times in different turbulent flows. The mean stretching rate obtained from (22) by taking the ensemble average over $10 \times N^2$ chopped lines is drawn with a solid curve in figure 4(b). After a transient period ($t \lesssim 10\,\overline{\tau}_\eta$) it settles down around $0.17\,\overline{\tau}_\eta{}^{-1}$ in the mean, which agrees with (15) as expected. A dotted curve is for the thin-tube average which is replotted from figure 4(a) for comparison. The thin-tube average underestimates the line average by 24%. The gray zone represents the standard deviation of the stretching rate over the ten realizations, which is also stationary in time. The mean standard deviation averaged over $t/\tau_\eta = 20 \sim 90$ is $0.01\,\overline{\tau}_\eta{}^{-1}$.

3.5 Stretched Factor — A Bridge between Line Average and Thin-Tube Average

The underestimation of the stretching rate by a simple volume average described in Sec. 3.3 is originated from the negligence of the non-uniform probability weight by the non-uniform stretching of lines. As seen in the expression (20), the weight factor is the segment length $l_t^{*(j)}$ ($j = 1, 2, \cdots, I^*$) itself at time t. We normalize the weight factor by their initial lengths l_0^* *which are common to all the segments* as

$$\sigma_t^{*(j)} = \frac{l_t^{*(j)}}{l_0^*} = \exp\left[\int_0^t \gamma_{t'}^{*(j)} \mathrm{d}t'\right] \qquad (j = 1, 2, \cdots, I^*)\,, \tag{24}$$

and call $\sigma_t^{*(j)}$ the stretched factor. The second equality of (24) has been derived by the integration of (21). Then, the overall stretching rate of lines is written, by using (19) and (20), as

$$\gamma_{\mathrm{L}} = \frac{\sum_{j=1}^{I^*} \sigma_t^{*(j)}\, \gamma_t^{*(j)}}{\sum_{j=1}^{I^*} \sigma_t^{*(j)}} = \frac{\langle \sigma^* \gamma^* \rangle_{P_t}}{\langle \sigma^* \rangle_{P_t}}. \tag{25}$$

where the brackets $\langle\ \ \rangle_{P_t}$ denotes the probability average with respect to the joint probability density function (PDF) $P_t(\sigma^*, \gamma^*)$ of the stretched factor σ_t^* and the stretching rate γ_t^* of segments of a common initial length

$$\begin{aligned} \langle f \rangle_{P_t} &= \int_0^\infty \mathrm{d}\sigma^* \int_{-\infty}^{\infty} \mathrm{d}\gamma^*\, f(\sigma^*, \gamma^*)\, P_t(\sigma^*, \gamma^*) \\ &= \frac{1}{I^*} \sum_{j=1}^{I^*} f(\sigma_t^{*(j)}, \gamma_t^{*(j)}) \end{aligned} \tag{26}$$

This is exactly the thin-tube average so that the probability average is equivalent to the thin-tube average, i.e

$$\langle f \rangle_{P_t} = \langle f \rangle_{\mathrm{tube}}\,. \tag{27}$$

If σ_t^* and γ_t^* were statistically independent of each other, then $\langle \gamma^* \sigma^* \rangle_{P_t} = \langle \gamma^* \rangle_{P_t} \langle \sigma^* \rangle_{P_t}$ and the mean stretching rate of lines would be given by $\langle \gamma^* \rangle_{P_t}$, i.e., the thin-tube average. If, on the other hand, they are positively correlated as it is the case, the ratio (25) should be greater than the thin-tube average. In figure 5, we plot the joint PDF $P_t(\sigma^*, \gamma^*)$ at time $20\,\overline{\tau}_\eta$, where the abscissa and the ordinate are normalized by the mean values of the respective quantities. The contours are elongated upper-right, and the conditional average, which is drawn with a solid curve, of γ^* for a given σ^* increases with σ^*. These indicate that σ^* and γ^* are indeed positively correlated. In fact, we find that $\langle \sigma^* \gamma^* \rangle_{P_t} = 2.82\,\overline{\tau}_\eta{}^{-1}$, $\langle \sigma^* \rangle_{P_t} = 17.6$, and $\langle \gamma^* \rangle_{P_t} = 0.12\,\overline{\tau}_\eta{}^{-1}$, so that

$$\frac{\langle \sigma^* \gamma^* \rangle_{P_t}}{\langle \sigma^* \rangle_{P_t}} = 0.16\,\overline{\tau}_\eta{}^{-1} > \langle \gamma^* \rangle_{P_t} = 0.12\,\overline{\tau}_\eta{}^{-1}\,. \tag{28}$$

The values 0.16 and 0.12 agree, within numerical uncertainty, with 0.17 in (15) and 0.13 in (18), respectively. The same behavior is observed at any times after $20\,\overline{\tau}_\eta$.

We have seen that both the line average and the thin-tube average of the stretching rate γ_t of passive lines are calculated by the use of the joint PDF of γ_t and the stretched factor σ_t. This is applied to any physical quantity accompanied with fluid elements. In this sense the stretched factor works as a bridge to relate the two different averages.

3.6 Weighted Volume Average

The results of the preceding section encourage us to calculate the joint PDF $P_t(\sigma, \gamma)$ in the passive-vector-element simulation described in Sec. 3.3, because we can then estimate the correct stretching rate of passive lines through (25). In this section we shall show that it is indeed possible, but there is a severe restriction in keeping the numerical accuracy.

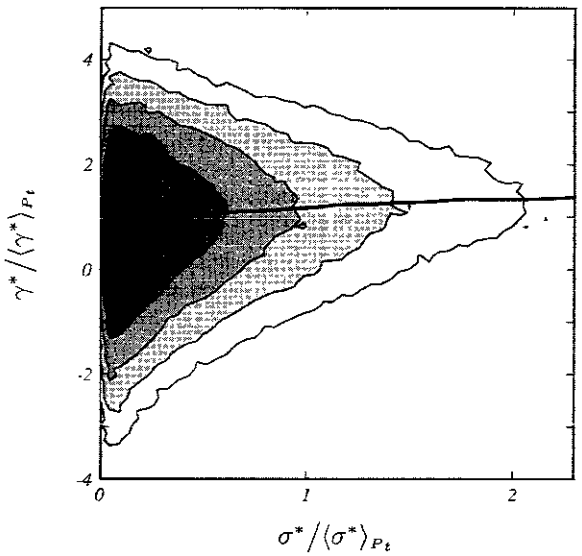

Figure 5 Joint PDF of the stretched factor σ^* and the stretching rate γ^*. The PDF takes larger values in darker areas. The contour levels are 0.02, 0.04, 0.08, 0.16, and 0.32. Solid line denotes the conditional average γ^* for a given σ^*. The abscissa and the ordinate are normalized by the probability averages $\langle\sigma^*\rangle_{P_t} = 17.6$ and $\langle\gamma^*\rangle_{P_t} = 0.12\,\overline{\tau}_\eta^{-1}$, respectively. $t = 20\,\overline{\tau}_\eta$.

To do this we calculate the stretched factor $\sigma_t^{(i)}$ of each element $\delta\boldsymbol{l}^{(i)}$ $(i = 1, 2, \cdots, N^3)$ in addition to the stretching rate $\gamma_t^{(i)}$ in the passive-vector-element simulation. Under the uniform mixing hypothesis the formula (25) of the mean stretching rate of passive lines formulated on lines may be extended, at sufficiently later times, to the weighted volume average,

$$\langle\gamma\rangle_{\mathrm{vol/w}} = \frac{\sum_{i=1}^{N^3}\gamma_t^{(i)}\sigma_t^{(i)}}{\sum_{i=1}^{N^3}\sigma_t^{(i)}}\,. \tag{29}$$

The mean stretching rate obtained by the ensemble average over 25 realizations, namely, over $25 \times N^3$ vector elements, is plotted against time with a thin curve in figure 4(c). The gray zone represents the standard deviation. The mean stretching rate in the line average is shown with a thick curve for comparison. They agree very well with each other at the early stage of evolution ($t < 0.8\,\overline{\tau}_\eta$, say), but then the thin curve deviates slightly upward and stays steadily above the thick curve throughout all the subsequent times. The mean stretching rate averaged over the period $20\,\overline{\tau}_\eta \le t \le 90\,\overline{\tau}_\eta$ is found to be

$$\langle\gamma\rangle_{\mathrm{vol/w}} = 0.18\,\overline{\tau}_\eta^{-1}. \tag{30}$$

As seen above, the estimation of the stretching rate of passive lines by the weighted volume average indeed gives the correct value at early stages of evolution, but suffers from overestimation after about ten Kolmogorov times. The amount of the overestimation does not increase in time but stays around 6% of the true value. In the following we consider the reason of these characteristics of the weighted volume average by the passive-vector-element simulation. We compare the formula (25) in the line simulation and its counterpart,

$$\langle\gamma\rangle_{\mathrm{vol/w}} = \frac{\sum_{i=1}^{I_0}\gamma_t^{(i)}\sigma_t^{(i)}}{\sum_{i=1}^{I_0}\sigma_t^{(i)}}\,. \tag{31}$$

in the passive-vector-element simulation starting with a straight row of I_0 $(= N)$ parallel vector elements. Recall that this passive-vector-element simulation is nothing but a line simulation without inserted segments (Sec. 3.3) so that the summands in (31), which are composed of the initial segments, are subsets of the corresponding ones in (25). Hence, the origin of the overestimation of the weighted volume average should be attributed to the difference between the full and partial summations appearing in these equations.

Now let us begin by considering the sums of the stretched factor on the denominators. Variations of the stretched factor along a passive line obtained by the line simulation are shown in figures 6 (a) and (b). Here, the values on three hundreds consecutive segments of the line at (a) $t = 5\,\overline{\tau}_\eta$ and (b) $t = 20\,\overline{\tau}_\eta$ are plotted with a succession of steps of width $l_t^{(i)}/\sigma_t^{(i)}$ $(0 \le i \le I_t)$, the initial length of the i-th segment. The number I_t of the segments over the whole line is 300 at $t = 5\,\overline{\tau}_\eta$ and 3,598 at $t = 20\,\overline{\tau}_\eta$. Therefore, the abscissa spans the whole line in (a), but only the 8.3% in (b). Observe that even the narrowest peak is composed of more than ten steps irrespective of time, which suggests that the step-width is sufficiently small to represent the variation of the stretched factor at all times. The area below these steps over the whole line gives the sum $\sum_{J=1}^{I^*}\sigma_t^{*(J)}$. The positions of the initial segments are denoted by dots. Adjacent pairs of dots are separated by l_0. The sum $\sum_{i=1}^{I_0}\sigma_t^{(i)}$ is equal to the area below a succession of shaded steps of width l_0 over the whole line. The row of dots seem to be marginally dense to represent the variation of the stretched factor in (a) but too sparse in (b). A single peak contains at least five dots and the shaded area approximates well the true area in (a). On the other hand, each shaded step typically covers a few peaks and the shaded area is greater than the true one in (b). This overestimation of the area is enhanced in proportion to the ratio of the step-width and the peak-width of the stretched factor.

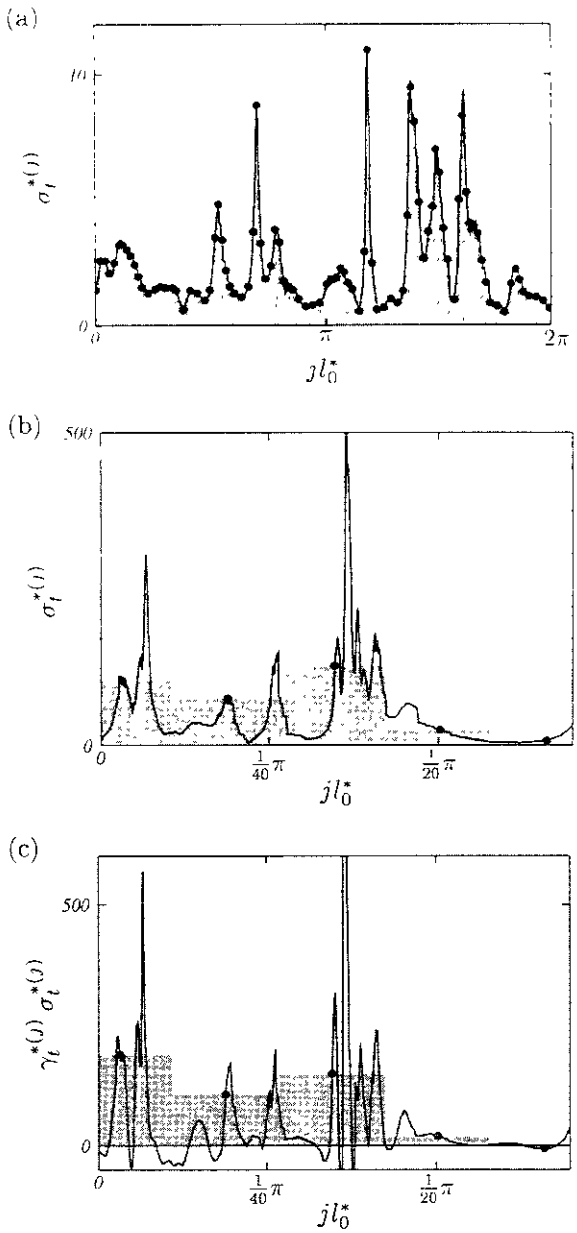

Figure 6 Overestimation of the area by sparse samples. (a) Variations along a passive line of the stretched factor at $t = 5\,\overline{\tau}_\eta$. The stretched factor on three hundreds of consecutive segments are drawn with a succession of solid steps of width of $l_t^{(i)}/\sigma_t^{(i)}$, the initial length of the i-th segment. The positions of the initial segments are designated with dots. The distance between adjacent dots is l_0. The area below a succession of steps of width of l_0 with dots at the center of each step is shaded. The shaded area is approximately the same as that below the solid steps. (b) Same as (a) but at $t = 20\,\overline{\tau}_\eta$. The shaded area is wider than that below the solid steps. (c) Same as (b) but for the product of the stretching and the stretched factor. The area below the shaded steps is wider than that below the solid steps. This overestimation is stronger than that in (b).

The same inequality also holds between the sums, $\sum_{j=1}^{l^*} \gamma_t^{*(j)}\sigma_t^{*(j)}$ and $\sum_{i=1}^{l_0} \gamma_t^{(i)}\sigma_t^{(i)}$, of the product of the stretching rate and the stretched factor on the numerators in (25) and (31). In figure (c), we plot the variation of the product on the same part of the line and at the same time as (b). It is seen that the product exhibits sharper peaks than the stretched factor as anticipated from the positive correlation between these two quantities (see figure 5). More precisely, while their widths are comparable between the two, the peaks of the product are higher than those of the stretched factor itself. This leads to an enhanced overestimation between the sums on the numerators stronger than that on the denominators in (25) and (31), which in turn results in the overestimation of $\langle\gamma\rangle_{\mathrm{vol/w}}$ compared with $\langle\gamma\rangle_{\mathrm{line}}$. Furthermore, since the correlation between the stretching rate and the stretched factor is stationary (see Sec. 3.5), the amount of this overestimation should also be invariant in time.

In conclusion, the deviation at later times of the weighted volume average is caused by the numerical scheme itself of the passive-vector-element simulation. Recall that the vector elements which represent passive line elements separate with each other exponentially in time. As soon as the distance between the neighboring elements becomes comparable with the length-scale of the variation of the rate-of-strain tensor, these dilute samples of the vector elements may not be able to approximate well the line statistics any more. In fact, the characteristic length of the variation of the rate-of-strain tensor is $O(10\overline{\eta})$ along a passive line, and the typical distance between the neighboring vector elements at time $10\,\overline{\tau}_\eta$, around which the deviation starts, is $8.4\,\overline{\eta}$. Here, the length scale of the latter has been estimated from the mean stretched factor $\exp[0.17 \times 10] (= 5.5)$ multiplied by the initial distance $\Delta x (= 1.5\overline{\eta})$ of the neighboring vector elements. Hence, the exponential increase of the distance between the neighboring elements gives a very severe constraint that makes the practical estimation by the passive-vector-element simulation almost impossible.

3.7 Statistics of Rate-of-Strain Tensor

In the preceding five sections we have seen that quite different values of the mean stretching rate of passive lines were obtained by different averaging. In order to understand the origin of the difference we examine here the statistics of the rate-of-strain tensor which directly determines the stretching rate. As seen in (17), the stretching rate of a vector element $\delta\boldsymbol{l}$ depends both on the rate-of-strain tensor $\underline{\boldsymbol{S}}$ and on the direction of $\delta\boldsymbol{l}$. In terms of the eigenvalues s_1, s_2, s_3 $(s_1 \geq s_2 \geq s_3)$ of $\underline{\boldsymbol{S}}$, and the angles α_1, α_2, α_3 between $\delta\boldsymbol{l}$ and each of the three principal axes of $\underline{\boldsymbol{S}}$, the stretching rate is expressed

by

$$\gamma_{\delta l} = s_1 \cos\alpha_1 + s_2 \cos\alpha_2 + s_3 \cos\alpha_3. \qquad (32)$$

If all the vector elements δl are distributed isotropically independent of an incompressible velocity field, the mean stretching rate vanishes because $\langle \cos\alpha_1 \rangle = \langle \cos\alpha_2 \rangle = \langle \cos\alpha_3 \rangle$ and $s_1 + s_2 + s_3 = 0$. This is the reason why $\langle \gamma \rangle$ starts from the origin (see figure 4). The correlation must be established between the rate-of-strain tensor and the direction of passive vector elements for the non-zero stretching of passive lines to show up. In the following the PDFs of the strength of the rate-of-strain tensor and the alignment angles with passive vector elements will be examined.

The PDFs in three different statistics of the second invariant $s^2 = {s_1}^2 + {s_2}^2 + {s_3}^2$ of the rate-of-strain tensor averaged over $20 \leq t/\tau_\eta \leq 50$ are compared in figure 7. The thick and thin solid curves denote the PDFs in the line and the thin-tube statistics, respectively. Difference between these two curves is substantial. Larger values of s^2 is less probable in the thin-tube statistics, that is, those elements having higher strain rate are less weighted because of depopulation by stretching (see figure 1(b) also). This is the reason of underestimation of the mean stretching rate in the thin-tube statistics.

A dotted curve that lies on the thin solid curve represents the PDF obtained by the Eulerian volume statistics, i.e. a simple summation of the contribution from each grid point. The perfect coincidence of these two curves provides us with a strong support to the uniform mixing hypothesis that samples restricted on passive lines and those chosen from the entire flow field give the same statistics. In other words, the Eulerian and the Lagrangian volume averages are equivalent.

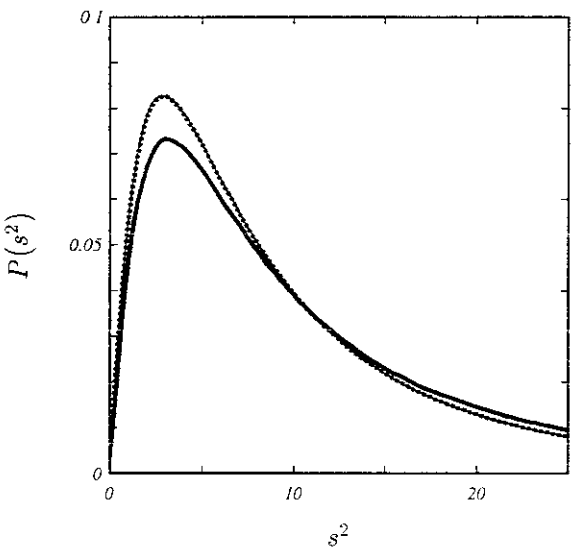

Figure 7 PDFs of the second invariant s^2 of the rate-of-strain tensor. A thick, a thin, and a dotted curves refer to the line statistics, the thin-tube statistics, and the Eulerian volume statistics, respectively. Averaged over $20 \leq t/\tau_\eta \leq 50$.

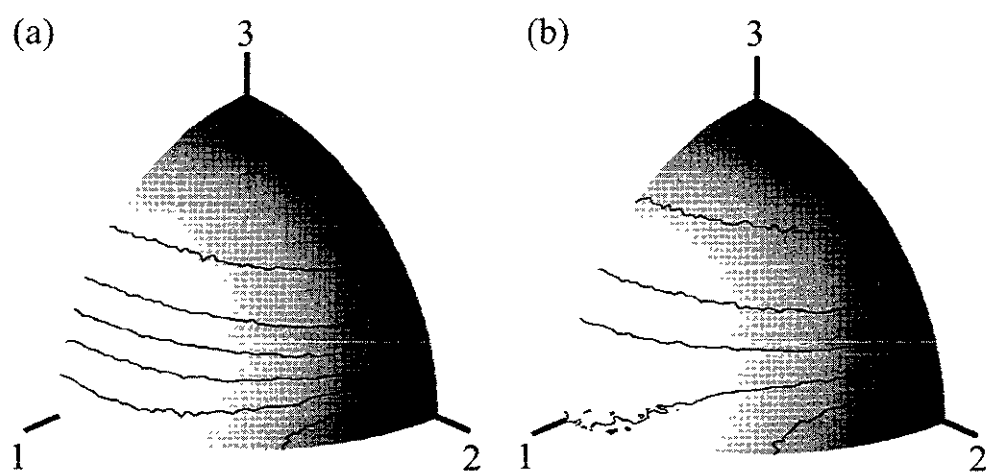

Figure 8 PDF of the angles between passive vector elements and the three principal axes of the rate-of-strain tensor. The number attached with each axis denotes the directions of the first, the second, and the third principal axes. The levels of contours are 0.25, 0.50, 0.75, 1, 1.25, and 1.5 from the top line. Averaged over $20 \leq t/\tau_\eta \leq 50$. (a) Line statistics. (b) Thin-tube statistics.

The alignment between the passive vector elements and the principal axes of the rate-of-strain tensor is also different between the line statistics and the thin-tube statistics. In figures 8, we plot the PDFs of the direction of vector elements relative to the three principal axes of the rate-of-strain tensor averaged over $20 \leq t/\overline{\tau}_\eta \leq 50$ in (a) the line statistics and (b) the thin-tube statistics. The numbers attached to the coordinate axes denote the principal axes. The contour levels are 0.25, 0.50, 0.75, 1, 1.25, and 1.5 from the top line. The segments tend to be aligned with a plane spanned by the first and the second principal axes in the line statistics more than the thin-tube statistics. This alignment to larger strain direction also contributes to the enhancement of line stretching. Incidentally, the most probable alignment of the passive vector elements to the second principal axis may be rephrased that they tend to be directed toward the local vorticity because the vorticity vectors are strongly aligned with this axis [5].

4 Concluding Remarks

In an incompressible flow, the number density of passive (or Lagrangian) particles in a passive volume remains uniform if it was so at the initial time. Therefore, the conditional mean of any physical quantity accompanied with fluid elements over a passive volume may be calculated by averaging the equi-weight contribution from each particle in this volume. For example, the mean enstrophy (vorticity squared) in a homogeneous turbulent flow evaluated by the average at all the uniform grid points is the same as that evaluated at all the passive particles leaving at each grid point. However, the number density of passive particles is generally not uniform on a passive line or on a passive surface even if it was so initially, because of non-uniform stretching of one- or two-dimensional objects. Hence, the mean stretching rate of lines or surfaces evaluated by the arithmetic mean of the contribution (without statistical weight due to the non-uniform stretching) from the passive line or surface elements does not give the correct answer.

The correct statistics on a passive line is the main theme of the present paper. We have introduced two similar but different averages: the line average and the thin-tube average (figure 1). Both of them are defined by the limit of vanishing diameter of the volume average over a thin tube including a passive line, but the way of choice of the tube is quite different between the two. In the former a tube of uniform diameter is chosen which includes a passive line at every time when the average is taken, whereas in the latter it is a passive tube which evolves from a uniform tube already set up at an earlier time. Note that the tube diameter can be non-uniform at the time of averaging in the latter, which leads to a substantial difference between the two statistics. The line average is the correct one, by the way.

A simple arithmetic average over passive particles which started on a line is nothing but the thin-tube average whereas the line average is obtained by taking account of the statistical weight (the stretched factor), which is proportional to the distance between adjacent particles, to the contribution from each particle. Here, it is important to keep in mind that adjacent pairs of particles should always be kept sufficiently close, e.g. within the order of the Kolmogorov length, in numerical simulations for the accurate estimation of the line statistics. Since a passive line migrates uniformly in a stationary and homogeneous turbulent flow (the uniform mixing hypothesis), the statistics of passive particles which started on a line is the same as those of passive particles floating uniformly over the whole flow field. In other words, the thin-tube statistics and the Lagrangian volume statistics are the same in the well mixed region (figure 4(a)). Based on this concept, the Lagrangian volume statistics over the passive particles with associated direction (i.e. the passive vector elements) were employed in previous studies [3, 4] to estimate the mean stretching rate of passive lines. However they underestimated (see figure 4(b)) the stretching rate of passive lines because of the neglection of the fact that the number density of particles is lower but the stretching rate is higher where a passive line has been more stretched. The correct value would be recovered at least in the early stage of evolution if the stretched factor were taken into account in averaging (figure 4(c)). However, the accuracy is deteriorated rapidly because of an exponential increase of the mutual distance between initially neighboring vector elements (Sec. 3.6). That is, as soon as the distance becomes comparable with the length scale of variation of the rate-of-strain tensor, which is $O(10\eta)$, the accuracy may decline quite rapidly and the mean stretching rate is likely to be overestimated (by 6% in the present case). This implies that the accurate estimation of the stretching rate of passive lines is practically impossible by the passive-vector-element simulation and that a true line simulation as described in Sec. 3.2 is necessary.

A similar relation between the line and the thin-tube statistics (Sec. 2) also holds in the surface statistics. The *surface average* may be expressed by the limit of volume average of a physical quantity $F(\boldsymbol{x}, t)$ over a layer V_t of uniform thickness $\mathrm{wid}(V_t)$ as

$$\langle F \rangle_{\mathrm{surf}} = \lim_{\mathrm{wid}(V_t)\to 0} \frac{1}{V_t} \int_{V_t} F(\boldsymbol{x}, t) \mathrm{d}V. \qquad (33)$$

On the other hand, the *thin-layer average* is defined by the thin limit of the volume average over a passive layer whose thickness is uniform at the initial time as

$$\langle F \rangle_{\mathrm{layer}} = \lim_{\mathrm{wid}(V_0)\to 0} \frac{1}{V_t} \int_{V_t} F(\boldsymbol{x}, t) \mathrm{d}V, \qquad (34)$$

where $\mathrm{wid}(V_0)$ denotes the thickness of the initial layer. Note that the thickness of the layer V_t is non-uniform

in general so that the surface average and the thin-layer average are different from each other, i.e.

$$\langle F \rangle_{\rm surf} \neq \langle F \rangle_{\rm layer} \,. \tag{35}$$

This disagreement between the two averages should be kept in mind when statistics of various physical quantities on interfaces of different fluids is studied.

Acknowledgements

This work has been partially supported by Grant-in-Aid for Scientific Research on Priority Areas (B) from the Ministry of Education, Science, Sports and Culture of Japan.

References

[1] N. Kasagi and K. Nishino, Experimental Thermal and Fluid Science **4**, 601 (1991).

[2] G. K. Batchelor, Proc. Roy. Soc. London A **213**, 319 (1952).

[3] S. S. Girimaji and S. B. Pope, J. Fluid Mech. **220**, 427 (1990).

[4] M.-J. Huang, Phys. Fluids **8**. 2203 (1996).

[5] M. T. Ashurst, A. R. Kerstein, R. M. Kerr, and C. H. Gibson, Phys. Fluids **30**, 2343 (1987).

Recent Issues of NIFS Series

NIFS-661 K Yamazaki, K Y Watanabe, A Sagara, H Yamada, S Sakakibara, K Narihara, K Tanaka, M Osakabe, K Nishimura, O Motojima, M Fujiwara, the LHD Group
Helical Reactor Design Studies Based on New Confinement Scalings, Sep 2000
(IAEA-CN-77/ FTP 2/12)

NIFS-662 I Hayashi, N Mizuguchi, H Miura and T Sato
Dynamics of Relaxation Phenomena in Spherical Tokamak, Sep 2000
(IAEA-CN-77THP2/13)

NIFS-663 H Nakamura and T Sato, H Kambe and K Sawada and I Saiki
Design and Optimization of Tapered Structure of Near-field Fiber Probe Based on FDTD Simulation, Oct 2000

NIFS-664 N Nakajima,
Three Dimensional Ideal MHD Stability Analysis in L=2 Heliotron Systems, Oct 2000

NIFS-665 S Fujiwara and T Sato,
Structure Formation of a Single Polymer Chain I Growth of trans Domains, Nov 2000

NIFS-666 S Kida,
Vortical Structure of Turbulence, Nov 2000

NIFS-667 H Nakamura, S Fujiwara and T Sato
Rigidity of Orientationally Ordered Domains of Short Chain Molecules, Nov 2000

NIFS-668 I Mutoh, R Kumazawa, T Seki, K Saito, Y Torii, F Shimpo, G Nomura, T Watari, D A Hartmann, M Yokota, K Akaishi, N Ashikawa, P deVries, M Emoto, H Funaba, M Goto, K Ida, H Idei, K Ikeda, S Inagaki, N Inoue, M Isobe, O Kaneko, K Kawahata, A Komori, T Kobuchi, S Kubo, S Masuzaki, T Morisaki, S Morita, J Miyazawa, S Murakami, T Minami, S Muto, Y Nagayama, Y Nakamura, H Nakanishi, K Narihara, N Noda, K Nishimura, K Ohkubo, N Ohyabu, S Ohdachi, Y Oka, M Osakabe, T Ozaki, B.J. Peterson, A Sagara, N Sato, S Sakakibara, R. Sakamoto, H Sasao, M Sasao, M Sato, T Shimozuma, M Shoji, S Sudo, H Suzuki, Y Takeiri, K Tanaka, K Toi, T Tokuzawa, K Tsumori, K Y Watanabe, T Watanabe, H Yamada, I Yamada, S Yamaguchi, K Yamazaki, M Yokoyama, Y Yoshimura, Y Hamada, O Motojima, M Fujiwara
Fast- and Slow-Wave Heating of Ion Cyclotron Range of Frequencies in the Large Helical Device, Nov 2000

NIFS-669 K Mima, M S Jovanovic, Y Sentoku, Z-M Sheng, M M Skoric and T Sato
Stimulated Photon Cascade and Condensate in Relativistic Laser-plasma Interaction, Nov 2000

NIFS-670 L Hadzievski, M M Skoric and T Sato
On Origin and Dynamics of the Discrete NLS Equation, Nov 2000

NIFS-671 K. Ohkubo, S Kubo, H Idei, T Shimozuma, Y Yoshimura, F Leuterer, M Sato and Y Takita,
Analysis of Oversized Sliding Waveguide by Mode Matching and Multi-Mode Network Theory, Dec 2000

NIFS-672 C Das, S Kida and S Goto,
Overall Self-Similar Decay of Two-Dimensional Turbulence, Dec. 2000

NIFS-673 L A Bureyeva, T Kato, V S Lisitsa and C Namba,
Quasiclassical Representation of Autoionization Decay Rates in Parabolic Coordinates, Dec 2000

NIFS-674 L A Bureyeva, V S Lisitsa and C Namba,
Radiative Cascade Due to Dielectronic Recombination, Dec 2000

NIFS-675 M.FHeyn, S V Kasilov, W Kernbichler, K Matsuoka, V V Nemov, S Okamura, O S Pavlichenko,
Configurational Effects on Low Collision Plasma Confinement in CHS Heliotron/Torsatron, Jan 2001

NIFS-676 K. Itoh,
A Prospect at 11th International Toki Conference - Plasma physics quo vadis?, Jan 2001

NIFS-677 S Satake, H Sugama, M Okamoto and M Wakatani,
Classification of Particle Orbits near the Magnetic Axis in a Tokamak by Using Constants of Motion, Jan 2001

NIFS-678 M Tanaka and A Yu Grosberg,
Giant Charge Inversion of a Macroion Due to Multivalent Counterions and Monovalent Coions Molecular Dynamics Studyn, Jan 2001

NIFS-679 K Akaishi, M Nakasuga, H Suzuki, M Iima, N Suzuki, A Komori, O Motojima and Vacuum Engineering Group,
Simulation by a Diffusion Model for the Variation of Hydrogen Pressure with Time between Hydrogen Discharge Shots in LHD, Feb 2001

NIFS-680 A Yoshizawa, N Yokoi, S Nisizima, S -I Itoh and K Itoh
Variational Approach to a Turbulent Swirling Pipe Flow with the Aid of Helicity, Feb 2001

NIFS-681 Alexander A.Shishkin
Estafette of Drift Resonances, Stochasticity and Control of Particle Motion in a Toroidal Magnetic Trap, Feb 2001

NIFS-682 H Momota and G H Miley,
Virtual Cathode in a Spherical Inertial Electrostatic Confinement Device, Feb 2001

NIFS-683 K Saito, R Kumazawa, T Mutoh, T Seki, T Watari, Y Torii, D A Hartmann, Y Zhao, A Fukuyama, F Shimpo, G Nomura, M Yokota, M Sasao, M Isobe, M Osakabe, T Ozaki, K Narihara, Y Nagayama, S Inagaki, K Itoh, S Morita, A.V Krasilnikov, K Ohkubo, M Sato, S Kubo, T Shimozuma, H Idei, Y Yoshimura, O Kaneko, Y Takeiri, Y Oka, K Tsumori, K Ikeda, A Komori, H Yamada, H Funaba, K Y Watanabe, S Sakakibara, M Shoji, R Sakamoto, J Miyazawa, K Tanaka, B J Peterson, N Ashikawa, S Murakami, T Minami, S Ohakachi, S Yamamoto, S Kudo, H Sasao, H Suzuki, K Kawahata, P deVries, M Emoto, H Nakanishi, T Kobuchi, N Inoue, N Ohyabu, Y Nakamura, S Masuzaki, S. Muto, K Sato, T Morisaki, M Yokoyama, T Watanabe, M. Goto, I Yamada, K Ida, T Tokuzawa, N Noda, S Yamaguchi, K Akaishi, A Sagara, K Toi, K. Nishimura, K Yamazaki, S Sudo, Y Hamada, O Motojima, M Fujiwara,
Ion and Electron Heating in ICRF Heating Experiments on LHD, Mar 2001

NIFS-684 S Kida and S Goto,
Line Statistics Stretching Rate of Passive Lines in Turbulence, Mar 2001